Energy & Buildings 356 (2026) 117083

Contents lists available at ScienceDirect

Energy & Buildings

journal homepage: www.elsevier.com/locate/enb

# Photothermal heating and solar harvesting through multiple transparent $Fe_3O_4$@$Cu_{2-x}S$ thin films with a solar dome

Meher Saketh Gandharapu [a], Anudeep Katepalli [a], Anton Harfmann [b], Mathias Bonmarin [c], John Krupczak [d], Donglu Shi [a,*]

[a] The Materials Science and Engineering Program, Department of Mechanical and Materials Engineering, College of Engineering and Applied Science, University of Cincinnati, Cincinnati, OH 45221, USA
[b] College of Design, Architecture, Art and Planning, University of Cincinnati, Cincinnati, OH 45221, USA
[c] School of Engineering, Zurich University of Applied Sciences, 8400 Winterthur, Switzerland
[d] Department of Engineering, Hope College, Holland, MI 49423, USA

ARTICLE INFO

*Keywords:*
Solar dome
Photothermal heating
Energy-neutral building
Photothermal tunnel
Utility

ABSTRACT

A novel building utility heating system is developed based on solar harvesting through multiple transparent photothermal (PT) panels arranged in a tunnel structure. Sunlight is collected by a rooftop solar dome and guided into a Photothermal Solar Tunnel (PTST), which achieves efficient conversion of solar radiation into thermal energy for passive heating. The PT panels are fabricated from thin films of $Fe_3O_4$@$Cu_{2-x}S$ plasmonic nanoparticles, which, due to localized surface plasmon resonance (LSPR), exhibit strong absorption in the UV and IR regions while maintaining minimal absorption in the visible band. This unique optical property enables high average visible transmittance (AVT), allowing sunlight to penetrate sequential panels within the PTST while the system functions as a transparent heat radiator. Controlled experiments under diverse environmental conditions, including extreme subzero temperatures, demonstrate the PTST's strong heating capability: interior tunnel surfaces reached above 30.9°C from ambient temperatures of −7°C with only minimal insulation. These results establish PTST as a scalable, cost-effective, and off-grid technology for sustainable building heating. By eliminating the need for complex solar system integration or bulky components, this approach opens a new pathway for passive solar energy utilization, advancing energy-neutral and environmentally resilient solutions for next-generation buildings.

## 1. Introduction

The U.S. Energy Information Administration (EIA) reports that space heating alone accounts for approximately 42% of household site energy consumption and nearly 32% of total energy use in commercial buildings [1]. This substantial energy demand, particularly in dense urban environments, underscores the urgent need for innovative building-scale heating technologies to meet global climate objectives, including the net-zero emissions target set at COP26 [2]. Reducing the energy footprint of building heating therefore remains a critical challenge at the intersection of materials science, architecture, and sustainable energy systems.

Among renewable energy technologies, photovoltaic (PV) solar systems and photothermal (are widely deployed across a broad range of applications [3–8]. Utility-scale solar installations can generate electricity for diverse energy needs, including building-related heating [9,10], and recent studies on transparent photothermal and smart semi-transparent window systems highlight alternative approaches for direct solar energy utilization. However, these systems typically require extensive land use, leading to conflicts with agriculture and residential development [11]. In addition, utility-scale PV systems involve complex infrastructure – including PV modules, inverters, mounting structures, transformers, and grid interconnections – which increases cost, installation complexity, and maintenance requirements. Solar thermal

*Abbreviations:* PTST, Photothermal Solar Tunnel; PT, Photo Thermal; PTP, Photo Thermal Panels; AVT, Average Visible Transmittance; LSPR, Localized Surface Plasmon Resonance; PE, Polyethylene; $Fe_3O_4$@$Cu_{2-x}S$, Magnetite-Copper sulfide; $Cu(acac)_2$, Copper Acetylacetonate; Q, Thermal Energy; ΔT, Temperature difference; m, Mass of the sample (thin film + substrate) (kg); Cp, Specific heat of panel substrate.

* Corresponding author.
*E-mail address:* shid@ucmail.uc.edu (D. Shi).

https://doi.org/10.1016/j.enbuild.2026.117083
Received 5 April 2025; Received in revised form 27 January 2026; Accepted 29 January 2026
Available online 31 January 2026

technologies for space heating face similar challenges, as many rely on opaque collectors, circulating heat-transfer fluids, thermal storage units, and active control components. These features limit their integration into building envelopes, introduce seasonal efficiency constraints, and complicate retrofitting with existing infrastructure.

Recent research efforts have explored alternative solar thermal strategies aimed at reducing system complexity while improving architectural compatibility. In particular, transparent and semi-transparent photothermal (PT) materials have emerged as a promising direction, enabling solar energy harvesting without fully obstructing visible light transmission. Our recent studies [12–16] have systematically advanced this field by developing plasmonic nanoparticle–based transparent photothermal coatings that combine broadband solar absorption with high visible transparency. These works demonstrate that iron oxide nanoparticle coatings can achieve strong absorption in the ultraviolet (UV) and infrared (IR) regions while maintaining visible transmittance as high as ~90% [13]. Collectively, Refs. [12–18] establish a materials and device platform for transparent photothermal energy conversion and represent, to the best of our knowledge, the most recent and comprehensive investigations in this emerging area.

To convey the main idea of the system, we introduce the concept of a Photothermal Solar Tunnel (PTST) coupled with a solar dome, as illustrated in Fig. 1. The solar dome collects sunlight from a wide range of angles and directs it into a tunnel containing multiple transparent photothermal panels, enabling cumulative heat generation while maintaining visible light transmission. This schematic provides an overview of the system and its operating principle; detailed descriptions of the panel structure, nanoparticle composition, fabrication, and working mechanisms are provided in the Methods section. This approach allows readers to understand the overarching concept and motivation in the Introduction without overloading it with technical specifics.

Building upon these developments, we introduce a new solar heating architecture that extends transparent photothermal concepts from individual panels to an integrated, building-scale system. As shown in Fig. 1a, transparent photothermal films containing $Fe_3O_4$@$Cu_{2-x}S$ nanoparticles are deposited on glass substrates and arranged in parallel in a tunnel structure. Since these films/substrates are transparent, light can penetrate them through the tunnel reaching the other end of the tunnel. As $Fe_3O_4$@$Cu_{2-x}S$ nanoparticles are highly photothermal due to localized surface plasmon resonance (LSPR) [19–21], they can convert photons to thermal energy efficiently resulting in rapidly increasing temperatures as shown the infrared image (Fig. 1a). Based on this concept, we can utilize a commercial solar tunnel by inserting multiple photothermal panels for harvesting solar light with a solar dome which can direct sunlight from a wide range of angles into the solar tunnel.

Fig. 1b shows a solar dome installed on a rooftop collects sunlight and directs it into a Photothermal Solar Tunnel (PTST) composed of multiple transparent photothermal panels arranged in parallel. Each panel is coated with plasmonic iron oxide nanoparticles developed in our prior work [12–16], enabling sequential light penetration and distributed heat generation across multiple layers. In contrast to conventional solar thermal systems, this approach requires no electrical power, no circulating fluids, and no large auxiliary components. The PTST functions as a passive thermal irradiator, converting solar radiation directly into usable heat with minimal system complexity.

Despite substantial progress in solar thermal and building-integrated energy technologies, existing approaches largely rely on opaque collectors, bulky thermal storage, or active system integration. As a result, their application in transparent architectural elements and energy-neutral building envelopes remains limited. Moreover, prior studies have not addressed how multiple transparent photothermal panels can be arranged to enable cumulative heating while preserving visible light transmission under realistic environmental conditions. To the best of our knowledge, the concept of a Photothermal Solar Tunnel utilizing multiple transparent plasmonic nanoparticle–based panels in a tunnel configuration has not been previously reported. This system-level design represents a distinct advance beyond material demonstrations, translating recent photothermal material innovations [12–16] into a scalable and practical solution for building utility heating.

## 2. Experimental procedure

### 2.1. Synthesis of $Fe_3O_4$@Cu2-xS nanoparticles

$Fe_3O_4$@Cu2-xS nanoparticles were synthesized following established protocols from the literature [19–25]. 60 mL of oleylamine was initially heated to 300°C under a nitrogen atmosphere. 700 mg of iron acetylacetonate was then dissolved in a mixture of oleylamine and N-methyl-2-pyrrolidone. This mixture was injected into the preheated oleylamine solution. The temperature was maintained at 300°C for 10 min to ensure complete reaction. Afterward, the solution gradually cooled to 70°C.

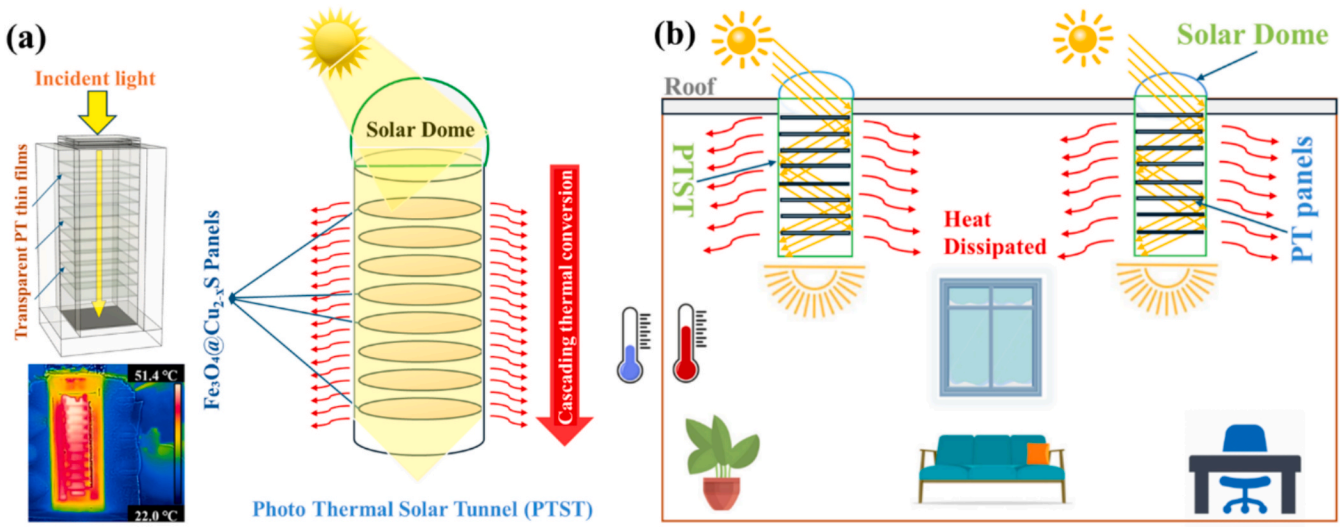


**Fig. 1.** (a) Schematic illustration of photothermal heating using multiple transparent $Fe_3O_4$@$Cu_{2-x}S$ thin films arranged in parallel. Infrared thermal imaging demonstrates efficient photon-to-heat conversion upon top-side solar irradiation.(b) Conceptual illustration of building utility heating using the Photothermal Solar Tunnel (PTST), in which a rooftop solar dome directs sunlight into a tunnel containing multiple transparent photothermal (PT) panels for passive, electricity-free heat generation.

Subsequently, 128.28 mg of sulfur dissolved in oleylamine, and cyclohexane was injected into the mixture. This was followed by the injection of 523.52 mg of copper acetylacetonate ($Cu(acac)_2$) dissolved in oleylamine and chloroform. The final solution was maintained at 70°C for 30 min. This sequential injection process facilitated the formation of $Fe_3O_4@Cu_{2-x}S$ nanoparticles. The nanoparticles were then washed three times with methanol to remove impurities, freeze-dried overnight, and stored in toluene for future use.

### 2.2. Fabrication of photothermal panels

Photothermal (PT) panels were fabricated by coating glass substrates (230 mm × 230 mm × 2.38 mm) with a nanoparticle-dispersed polymer solution. The coating solution was prepared by dispersing $Fe_3O_4@Cu_{2-x}S$ nanoparticles into an epoxy resin at a concentration of 1 mg/cm$^3$. The mixture was stirred thoroughly for 10 min to ensure uniform dispersion and to eliminate air bubbles. A total of 50 mL of the prepared polymer solution was applied to each glass panel by a doctor blade method [12], ensuring even distribution of nanoparticles across the surface. The coated panels were then cured at ambient temperature for 24 h.

### 2.3. Design of photothermal solar tunnel

The Photothermal Solar Tunnel (PTST) was constructed as depicted in Fig. 2a. The system includes a commercial solar dome (Sun Tek) at the top for solar harvesting, connected to a tunnel with a diameter of 35.56 cm and a height of 106 cm (Fig. 2b). Eight transparent PT panels were arranged vertically within the tunnel, with a uniform spacing of 5 cm; the first panel was positioned 5 cm below the base of the solar dome (Fig. 2c). The exterior of the dome was insulated with a thin polyethylene (PE) sheet to reduce heat losses, while the inner walls of the tunnel are lined with polished aluminum, exhibiting high total solar reflectance (0.85–0.95) with a predominantly specular component (Swift & Smith, 1995; Zhang & Muneer, 2002). This reflective lining efficiently directs sunlight through the tunnel, maintaining optical connectivity and enhancing light distribution across all panels. Temperature monitoring was conducted using K-type thermocouples: each PT panel was equipped with a central probe, and four additional thermocouples were positioned inside the tunnel at 100 cm, 80 cm, 60 cm, and 30 cm from the bottom, as indicated by the red dots in Fig. 2c, enabling detailed thermal profiling. The effectiveness of the reflective lining is quantitatively supported by the measured thermal performance, with the lowest panel reaching 46.1°C, consistent with light-transport predictions for high-aspect-ratio solar tubes (Callow, 2003). For future work, direct characterization of the specular-to-diffuse reflectance ratio could further refine optical modeling and improve predictive accuracy for thermal performance under varying solar incident angles and panel configurations.

## 3. Results

### 3.1. Characterization of the $Fe_3O_4@Cu_{2-x}S$ nanoparticles and thin films

The synthesis and characterization of $Fe_3O_4@Cu_{2-x}S$ nanoparticles and thin films have been previously reported [12,13,25,26]. Fig. 3 presents the characterization results of the transparent $Fe_3O_4@Cu_{2-x}S$ thin films. The transmission electron microscopy (TEM) image in Fig. 3a shows monodispersed nanoparticles with an average diameter of 15 nm. Spin-coating the nanoparticle solution onto a glass substrate resulted in uniform thin films [12]. Both photothermal heating curves and absorptions of the $Fe_3O_4@Cu_{2-x}S$ thin films have been previously reported [12,13,25–27]. The $Fe_3O_4@Cu_{2-x}S$ panel exhibits an average visible transmittance of 65% at a concentration of $9.45 \times 10^{-5}$ g/cm$^2$. Note that AVT of film is nanoparticle concentration dependent [13]. Fig. 3b shows a photograph of a $Fe_3O_4@Cu_{2-x}S$ film placed in front of a building at the University of Cincinnati, demonstrating its high transparency. This high AVT in the optical window is essential for PTST, enabling efficient solar light harvesting in confined 3D spaces. Fig. 3c shows the absorption spectra of both $Fe_3O_4@Cu_{2-x}S$ and $Fe_3O_4$ for comparison. As can be seen in this figure, $Fe_3O_4$ has a strong absorption in the UV range while $Fe_3O_4@Cu_{2-x}S$ exhibits a broad range of absorption in the infrared regions with a peak near 1200 nm. A particular characteristic of $Fe_3O_4@Cu_{2-x}S$ is the "U" shaped absorption with a minimum in the visible band rendering the thin film transparent. The average sizes of Fe3O4 and $Fe_3O_4@Cu_{2-x}S$ nanoparticles are respectively around 10 nm and 15 nm. Due to introduction of $Cu_{2-x}S$ into Fe3O4, there is a pronounced infrared (IR) absorption as shown in Fig. 3c, which is associated with Localized Surface Plasmon Resonance (LSPR) [15,16]. This IR absorption is particularly important for the PTST system in terms of enhanced transparency and photon-to-heat conversion.

### 3.2. Photothermal experiments

The photothermal experiments using the Photothermal Solar Tunnel (PTST) with a solar dome was conducted on August 4$^{rth}$, 2024, from 2 PM to 3:30 PM on the main campus of University of Cincinnati. The ambient temperature was 31 ∘C with all the conditions detailed in Fig. 4. Fig. 4a shows the experimental set up of PTST with a solar dome that allows solar light to fully penetrate the transparent photothermal panels to generate thermal energy. The heating curves are shown in Fig. 4b

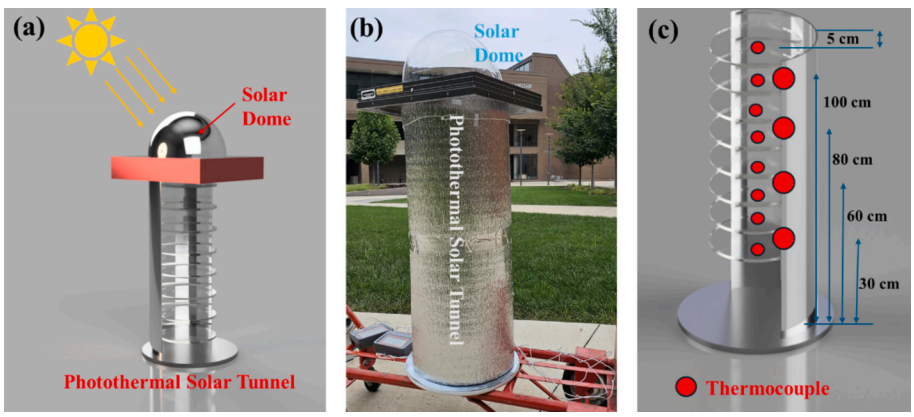


**Fig. 2.** (a) Schematic diagram of the Photothermal Solar Tunnel (PTST) system. (b) Photograph of the solar dome connected with the PTST. (c) The positions of thermocouples within the PTST as indicated by red spots. The small red dots are located right on the top of each PT panel in the center and the larger red circles are located right inside the PTST at heights of 100 cm, 80 cm, 60 cm, and 30 cm from the bottom of the tunnel, respectively. (For interpretation of the references to colour in this figure legend, the reader is referred to the web version of this article.)

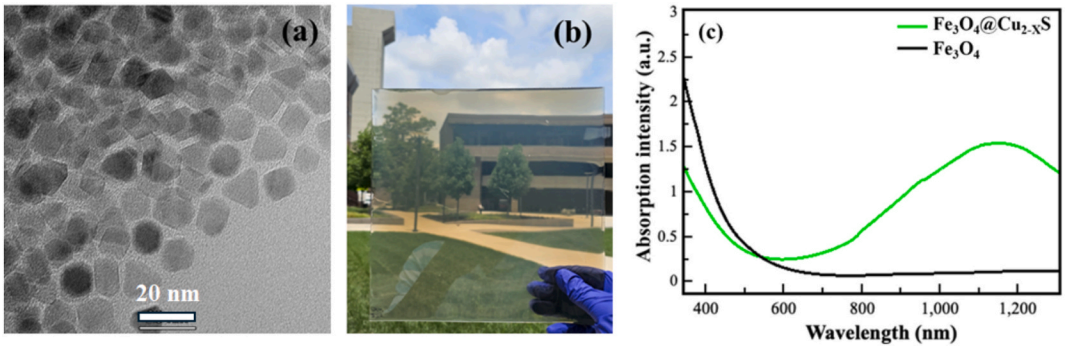


**Fig. 3.** (a) TEM image $Fe_3O_4@Cu_{2-x}S$ nanoparticles, (b) photograph of the $Fe_3O_4@Cu_{2-x}S$ thin film on glass substrate, and (c) optical absorption spectra of $Fe_3O_4@Cu_{2-x}S$ and $Fe_3O_4$.

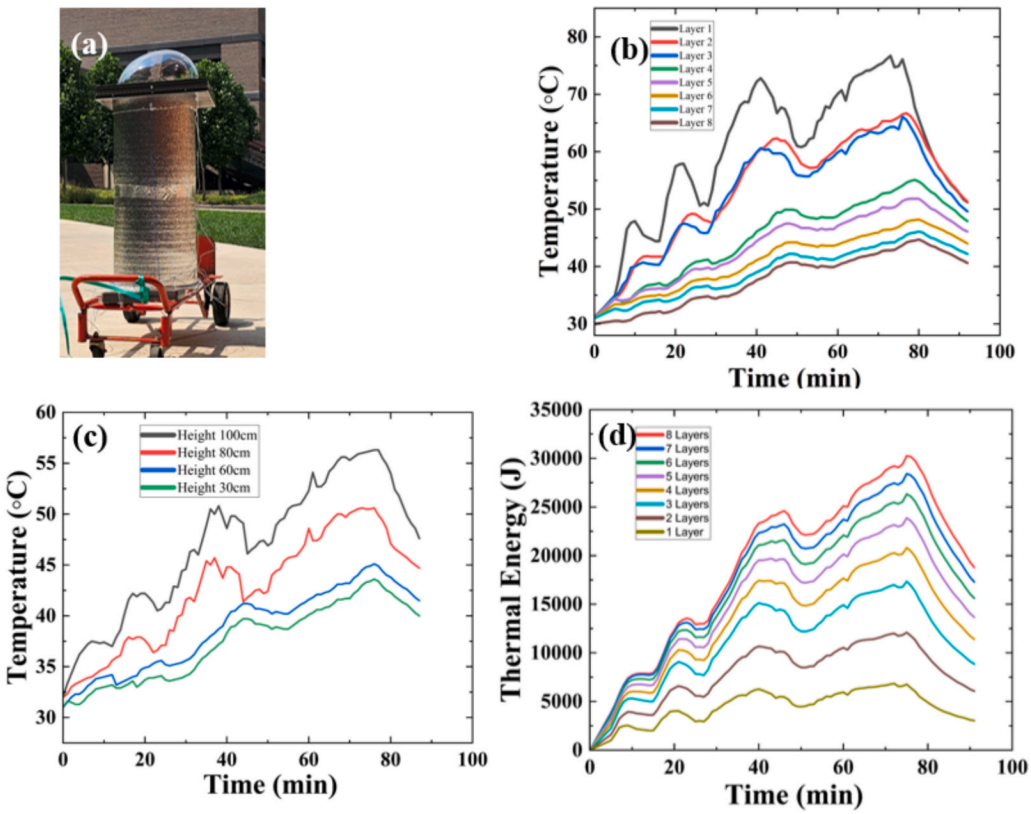


**Fig. 4.** (a) Photograph of Photothermal Solar Tunnel (PTST) on the main campus of University of Cincinnati for solar harvesting experiments. The experiments were conducted on August 4$^{rth}$, 2024 at 2 PM. Ambient temperature was 31°C. (b) Temperature vs time heating curves obtained from the thermocouples located on each photothermal panels as indicated by the red spots as shown in Fig. 2c. (c) Temperature vs time heating curves obtained from the thermocouples located inside the wall of PTST at heights of 100 cm, 80 cm, 60 cm, and 30 cm from the bottom of the tunnel, respectively. (d) Thermal energy vs time calculated from the heating curves. (For interpretation of the references to colour in this figure legend, the reader is referred to the web version of this article.)

with the thermocouples located on the top of each PT panel as depicted in Fig. 2c. As can be seen in this figure, the temperatures of all 8PT panels experience rapid increase initially and level off after 40 min forming plateaus until the sunlight is blocked at 80 min. As pointed by the arrows as shown in Fig. 2a, the incoming sunlight is at an angle into the solar dome. Under the weather conditions, due to cloud movements, the light intensity varies as reflected in the heating curves in Fig. 4b. Those valleys in top heating curves correspond to temporary clouds over the sky reducing the light intensity. This is characteristically different from the situation with the simulated solar light with constant light intensity [13]. After solar harvesting for 80 min, the system is moved under building shadow resulting in rapid fall of temperatures. As shown in Fig. 4b, the top three PT panels exhibit more pronounced variations in temperature, while the lower panels are more consistent due to the reduced light intensity at these levels. As shown in Fig. 4b, the highest temperature has reached 76.7°C (layer 1, grey), while the second top one (layer 2, red) is around 66.7°C. As also shown in Fig. 4b, even the lowest layer (layer 8, brown) has the highest temperature above 46.1°C indicating significant light penetration due to high AVT of the PT panels. Additionally, with the highly reflective aluminum interior of the solar tunnel, these lower panels can receive sufficient light for considerable photothermal effects.

Fig. 4c shows the temperature vs time for the thermocouple positions as depicted in Fig. 2c (large red circles). Note that these positions are located near the inside of the PTST wall at the heights of 100 cm, 80 cm, 60 cm, and 30 cm from the bottom of the tunnel, respectively. These

measurements were conducted to assess the temperature profiles of the entire tunnel. As can be seen in this figure, although the thermocouples are away from the photothermal films where the heating is most intensive, the top curve indicates the maximum temperature above 56.3°C, showing quite significant heating power. Even for positions far away from the top solar dome, the temperatures at 30 cm and 60 cm can reach above 43°C.

Thermal energy is defined as $Q = \Delta T_{max} \times m \times Cp$, where $\Delta T$ is the maximum temperature difference raised by a given number of thin films, m is the mass of the sample (thin film + substrate), and Cp is the specific heat of panel substrate (the PT films are extremely thin). The thermal energy is calculated based on the heating curves of the $Fe_3O_4@Cu_{2-x}S$ films installed in the PTST and plotted against the number of layers of PT panels. Fig. 4d illustrates the increase in heat energy generation with the addition of more PT panels (e.g., 1, 1 + 2, 1 + 2 + 3, etc.). For a single-layer system, the thermal energy generation is based on the heating curve of the top layer. For a two-layer system (1 + 2), the heating curves of both the top and second layers are used. Similarly, for a three-layer system (1 + 2 + 3), the thermal energy contribution from the top, second, and third layers is summed, and this pattern continues for additional layers. The thermal energy calculation considers only the heating curve, excluding the cooling curve, to emphasize the maximum heat energy generation across different layer configurations.

As shown in Fig. 4d, the thermal energy generated aligns with the heating curves in Fig. 4b. For a single panel in the PTST system, approximately 6800 J of thermal energy is produced over 75 min of heating. As additional panels are incorporated, the thermal energy generation increases proportionally, reaching up to 30000 J with a total of eight panels. This trend demonstrates a continuous rise in thermal energy accumulation. Given the cumulative nature of thermal energy generation, extended heating durations will result in even greater heat accumulation. With effective insulation and heat extraction from the PTST, it can be extrapolated that the system may generate up to 246000 J over 10 h of solar exposure.

Fig. 5a shows the experimental set up on October 2, 2024, at 2 PM under an ambient temperature of 21°C. Fig. 5b shows the temperature vs. time heating curves for all the PT panels, illustrating their thermal response over the experimental period. As expected, the top two panels (black and red) exhibited the highest temperature increase, reaching a peak temperature of 59.7°C, whereas the eighth panel recorded a lower maximum temperature of 38.3°C. This variation indicated light power density attenuation at different PT panels. The temperature variations at different heights along the tunnel wall are shown in Fig. 5c. As shown in Fig. 2c, the thermocouples were positioned at heights of 100 cm, 80 cm, 60 cm, and 30 cm for monitoring heat transfer within the tunnel. Based on the heating curves shown in Fig. 5b, the thermal energy generated are calculated. As shown in this figure, for a single panel, approximately 12700 J of thermal energy is produced over 90 min of heating. As the number of panels increases, the total thermal energy output scales accordingly, reaching up to 75,000 J when eight panels are utilized. This proportional increase indicates the scalability of the PTST system in thermal energy generation and its potential for enhanced performance with the integration of additional panels.

Another experiment was carried out on November 8, 2024, at 2 PM under an ambient temperature of 15°C (Fig. 6) which is considerably lower compared to the results shown in Fig. 5. It should be noted that the incident angle of solar light plays a critical role in determining the peak temperature attained by the system. As shown in Fig. 6c, the PTST

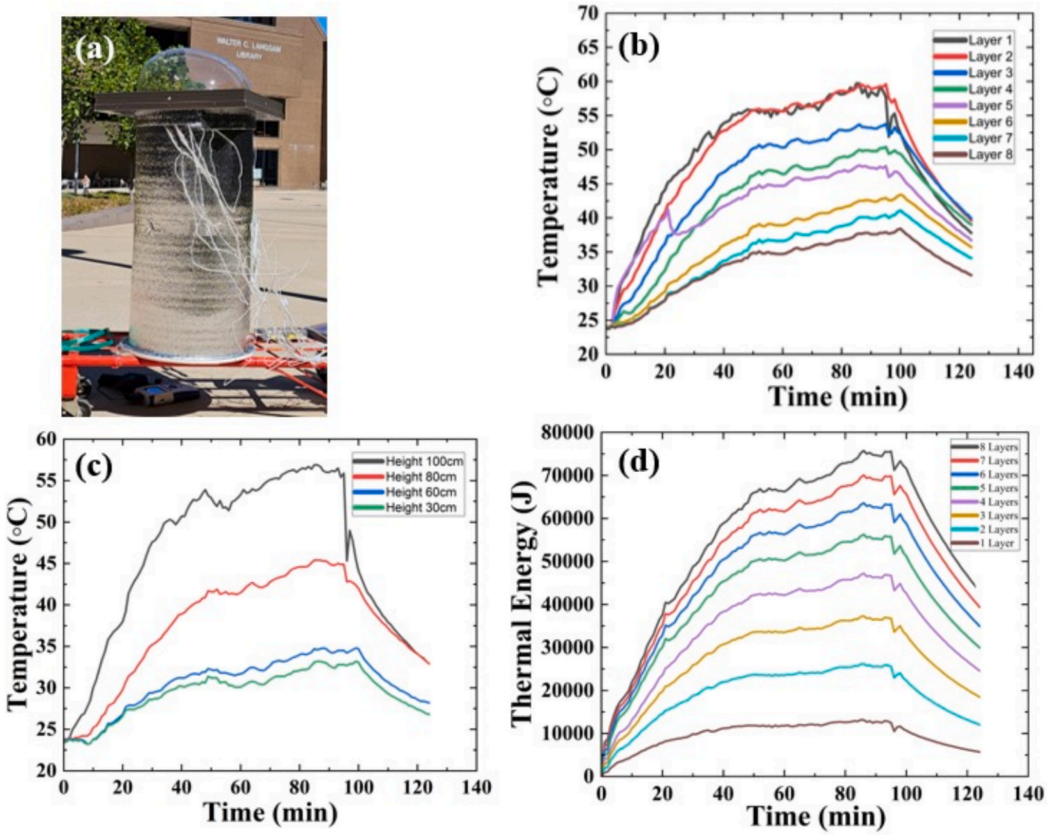


**Fig. 5.** (a) Photograph of Photothermal Solar Tunnel (PTST) on the main campus of University of Cincinnati for solar harvesting experiments. The experiments were conducted on October 2nd, 2024, at 2 PM. Ambient temperature was 21°C. (b) Temperature vs time heating curves obtained from the thermocouples located on each photothermal panels as indicated by the red spots as shown in Fig. 2c. (c) Temperature vs time heating curves obtained from the thermocouples located inside the wall of PTST at heights of 100 cm, 80 cm, 60 cm, and 30 cm from the bottom of the tunnel, respectively. (d) Thermal energy vs time calculated from the heating curves shown in Fig. 4b. (For interpretation of the references to colour in this figure legend, the reader is referred to the web version of this article.)

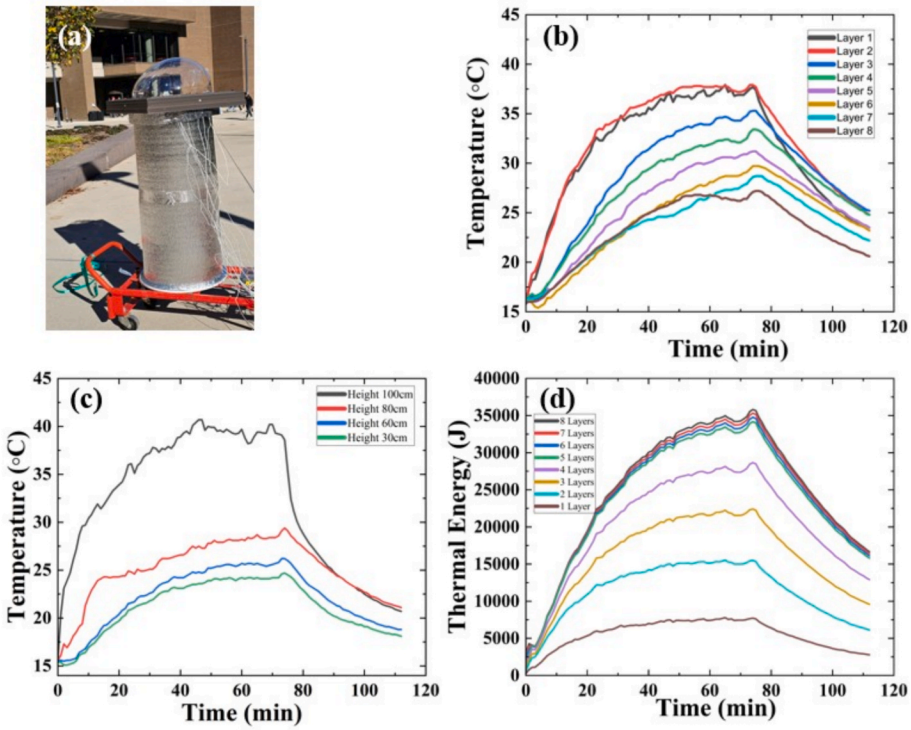


**Fig. 6.** (a) Photograph of Photothermal Solar Tunnel (PTST) on the main campus of University of Cincinnati for solar harvesting experiments. The experiments were conducted on November 8th, 2024, at 2 PM. Ambient temperature was 15 °C. (b) Temperature vs time heating curves obtained from the thermocouples located on each photothermal panels as indicated by the red spots as shown in Fig. 2c. (c) Temperature vs time heating curves obtained from the thermocouples located inside the wall of PTST at heights of 100 cm, 80 cm,60 cm, and 30 cm from the bottom of the tunnel, respectively. (d) Thermal energy vs time calculated from the heating curves shown in Fig. 4b. (For interpretation of the references to colour in this figure legend, the reader is referred to the web version of this article.)

system reaches the temperatures of 37.9°C and 27.2°C at 100 cm and 80 cm respectively. This large temperature gradient highlights the effects of heat dissipation and the thermal insulation efficiency of the stacked layers within the system. Furthermore, the total thermal energy generated under the lower ambient temperature conditions (15°C) is approximately 35,800 J for eight PT panels (Fig. 6d). This value is notably lower than the energy output recorded at 21°C in Fig. 5. This difference is attributable to the thin wall of the PTST system and can be well compensated with improved the thermal insulation.

To contextualize the trends observed in Fig. 6, it is instructive to consider representative magnitudes of incident-angle effects reported in the literature. Previous outdoor solar measurements have shown that light power density (LPD) incident on a fixed surface can decrease substantially over the course of the afternoon due to increasing solar incidence angles, with reported values dropping, for example, from approximately 48 mW/cm$^2$ to 30 mW/cm$^2$ between early and late afternoon hours. Such reductions highlight the sensitivity of measured irradiance to solar geometry rather than to intrinsic material performance.

A prolonged experiment was conducted on November 11, 2024, for 540 min (9 h) with even lower temperatures from 8 to 17 °C. During this period, the incident sunlight angle changed considerably resulting in building shadows covering the PTST system. To avoid shading effects, the PTST system was placed on a cart and moved to locations where it was under direct sunlight. As can be seen in Fig. 7b, there are temperature dips due to occasional cloud cover. Interestingly, the temperature dips can be observed on heating curves of all PT panels indicating consistent light power density variation and transmission of sunlight all the way to the bottom. The temperature variations are consistent at different heights of the thermocouples (100 cm, 80 cm, 60 cm, and 30 cm) as shown in Fig. 7c. Fig. 7d illustrates the accumulation of thermal energy over time, calculated from the heating curves in Fig. 7b. The thermal energy consistently increases throughout the experiment, reaching a peak of 93,700 J for a total of eight panels.

The performance of the Photothermal Solar Tunnel (PTST) system is primarily dictated by incident solar irradiance, as thermal generation depends on photon capture and conversion. The enclosed and semi-insulated design of the PTST – integrated within a building envelope – shields it from direct convective or advective influences such as wind or precipitation, ensuring that external airflow has minimal direct impact on the tunnel interior. However, transient atmospheric phenomena remain influential. Cloud cover, in particular, modulates system efficiency by attenuating incoming solar flux, leading to observable fluctuations in tunnel temperature. For example, the abrupt temperature variations presented in Fig. 7 correspond closely to intermittent cloud passages, which reduce photon delivery to the rooftop solar dome and thereby diminish photothermal output. While wind effects were largely mitigated by the enclosed tunnel structure, indirect influences such as enhanced convective heat losses from the solar dome or exterior surfaces under high wind conditions may contribute to overall system variability. In this study, systematic quantification of these broader meteorological effects was beyond scope, as the primary focus was on solar photon flux. Future work will incorporate detailed investigations of the coupled effects of cloud dynamics, wind speed, and other weather conditions to further evaluate and optimize PTST performance under real-world operating environments.

To be able to observe the seasonal effects on the photothermal heating capacity of PTST, we conducted solar harvesting experiments from summer to fall in 2024, and the latest ones were conducted in the winter of 2024 and spring of 2025. Fig. 8a shows the PTST experiment set up on the main campus of the University of Cincinnati on January 9, 2025, between 12:00 PM and 2:00 PM, a few days day after a heavy snow. The ambient temperature during the experiment ranged between −5°C and −7°C, providing a rigorous test of the PTST's performance

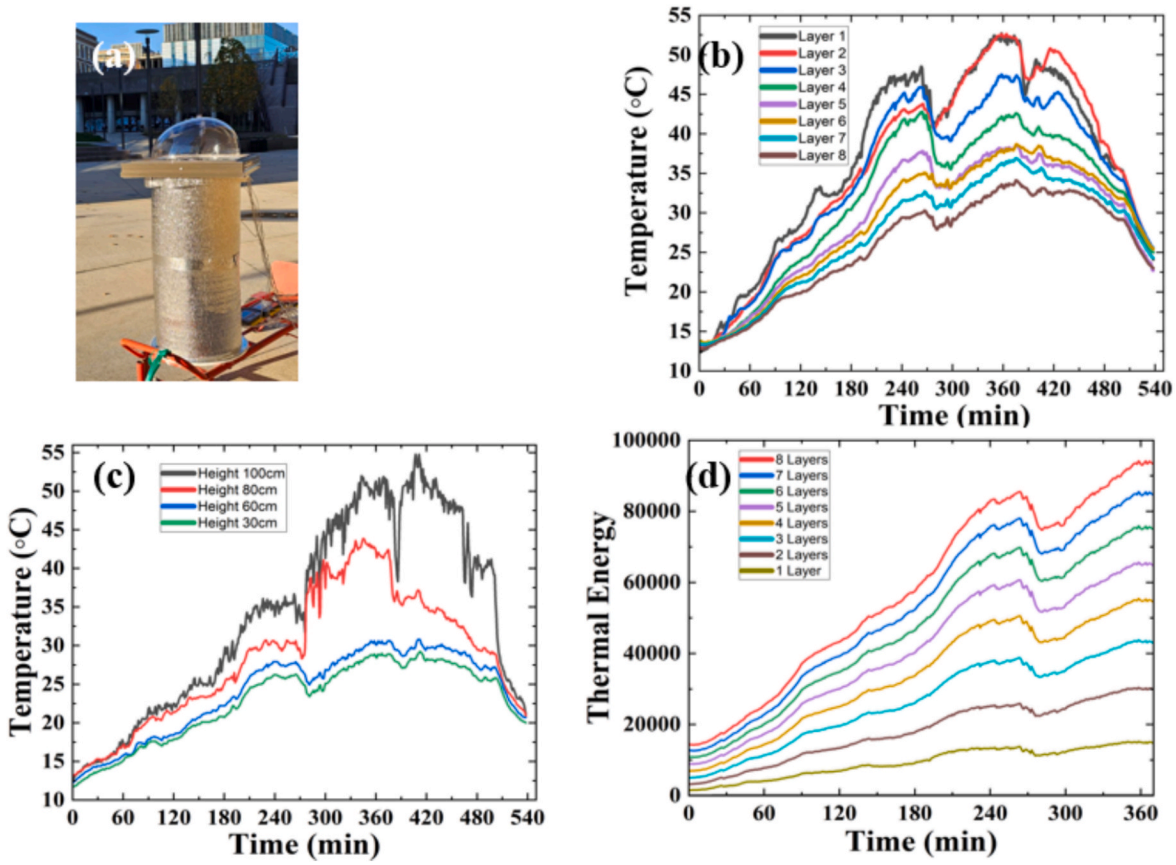


**Fig. 7.** (a) Photograph of Photothermal Solar Tunnel (PTST) on the main campus of University of Cincinnati for solar harvesting experiments. The experiments were conducted on November 11th, 2024, from 7:30 AM to 4:30 PM. Ambient temperature varied between 8 and 17 °C. (b) Temperature vs time heating curves obtained from the thermocouples located on each photothermal panels as indicated by the red spots as shown in Fig. 2c. (c) Temperature vs time heating curves obtained from the thermocouples located inside the wall of PTST at heights of 100 cm, 80 cm, 60 cm, and 30 cm from the bottom of the tunnel, respectively. (d) Thermal energy vs time calculated from the heating curves shown in Fig. 4b. (For interpretation of the references to colour in this figure legend, the reader is referred to the web version of this article.)

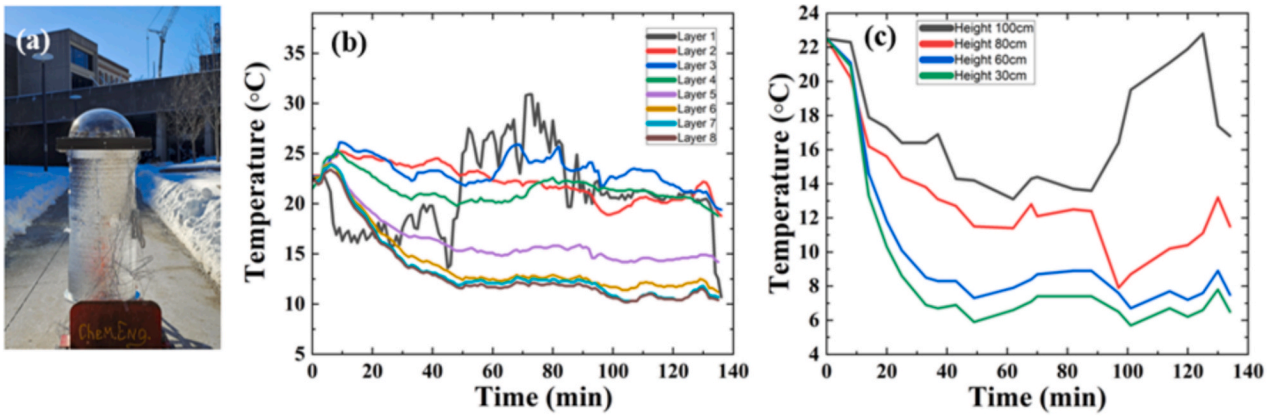


**Fig. 8.** (a) Photograph of Photothermal Solar Tunnel (PTST) on the main campus of University of Cincinnati for solar harvesting experiments. The experiments were conducted on January 9th, 2025 from 12 Noon to 2 PM. Ambient temperature varied between −5 to −7 ∘C. (b) Temperature vs time heating curves obtained from the thermocouples located on each photothermal panels as indicated by the red spots as shown in Fig. 2c. (c) Temperature vs time heating curves obtained from the thermocouples located inside the wall of PTST at heights of 100 cm, 80 cm, 60 cm, and 30 cm from the bottom of the tunnel, respectively. (For interpretation of the references to colour in this figure legend, the reader is referred to the web version of this article.)

under extreme cold conditions. Fig. 8b presents the temperature vs. time heating curves recorded from thermocouples positioned on each photothermal panel, as marked by the red spots in Fig. 2c. As a result of extremely low ambient temperatures, the heating curves indicate appreciable photothermal effects raising panel temperatures over 30.9°C at the top. It should be noted that the experimental setup was initially assembled indoors with room temperature around 22.8°C. Therefore, a gradual temperature drop was observed when the system was taken to outside. The photothermal heating took effect gradually, leading to a steady temperature rise. This highlights the system's rapid

thermal response and ability to function effectively even in freezing conditions.

The temperatures at different thermocouple heights are shown in Fig. 8c. As can be seen in this figure, the PT panel temperatures experience rapid decrease due to extremely low ambient temperature as the system was moved from the lab to outside the building. However, upon solar irradiation, the temperatures started to level off with the top panel (100 cm) temperature increasing to 22°C, demonstrating significant heat retention within the tunnel. Notably, despite subzero ambient temperatures, the photothermal panels efficiently maintained elevated temperatures inside the PTST, showing its effectiveness in mitigating heat loss. The findings in Fig. 8b and 8c reaffirm the strong photothermal heating performance of the PTST, even with only a thin polyethylene layer serving as thermal insulation. These results confirm the system's potential for practical applications in solar energy harvesting and passive heating, making it a viable solution for maintaining elevated temperatures in cold environments.

Fig. 9a shows the PTST installed on the main campus of the University of Cincinnati for solar harvesting experiments conducted on February 1st, 2025, from 12:00 PM to 2:20 PM. The ambient temperature during the experiment was 5°C, providing relatively mild conditions compared to previous tests as shown in Fig. 8. Note that the system was set up outside the building to provide the initial panel temperatures close to the ambient condition. Fig. 9b presents the temperature vs. time heating curves recorded from thermocouples placed on the photothermal panels, as indicated by the red spots in Fig. 2c. The data show a steady increase in temperature, with the second layer of the PT panel reaching a maximum temperature of 35°C. This demonstrates the system's effectiveness in capturing and converting solar energy into heat, despite low ambient temperature.

Fig. 9c shows consistent heating curves at thermocouple heights of 100 cm, 80 cm, 60 cm, and 30 cm from the bottom of the tunnel. As shown in this figure, at 100 cm, the temperature is approximately 24°C, suggesting that heat distribution within the tunnel is influenced not only by direct solar absorption but also by convection and radiative heat transfer from the PT panels. The thermal energy generated reveals a consistent increase in reaching a maximum of 63000 J (Fig. 9c). These experimental results indicate the effective photothermal heating performance of the PTST, even under cold winter conditions.

## 4. Discussion

The seasonal experimental results demonstrate the strong photothermal performance of the $Fe_3O_4$@$Cu_{2-x}S$ plasmonic coatings. These nanoparticles exhibit characteristic optical absorption peaks in the UV and IR regions, enabling efficient conversion of solar radiation into thermal energy under varying ambient conditions. Solar light, as a broad-spectrum electromagnetic wave, ideally should be harnessed efficiently by a solar harvesting device, converting most of the incident energy while maintaining high average visible transmittance (AVT). Fig. 10 shows the absorption spectrum of $Fe_3O_4$@$Cu_{2-x}S$, which exhibits a "U"-shaped profile with strong UV and broad IR absorption peaks, while allowing high visible light transmittance. The dashed line in Fig. 10 represents the ideal spectral pattern, achieving maximum UV and IR absorption with minimal attenuation in the visible range. Such high AVT allows sunlight to penetrate multiple PT panels along the full length of the Photothermal Solar Tunnel (PTST), enabling effective utility heating in large buildings. Strong UV and IR absorption ensures

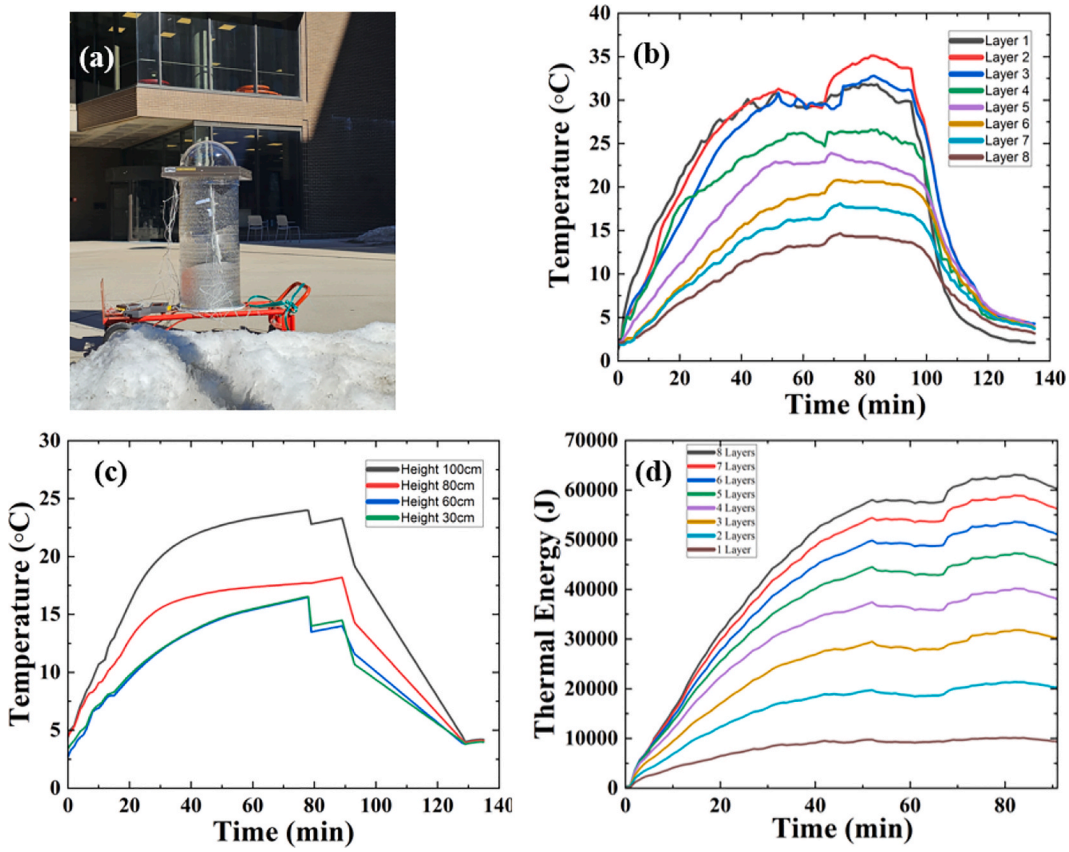


**Fig. 9.** (a)Photograph of Photothermal Solar Tunnel (PTST) on the main campus of University of Cincinnati for solar harvesting experiments. The experiments were conducted on February 1st, 2024, from 12 Noon to 2.20 PM. Ambient temperature was 5°C. (b) Temperature vs time heating curves obtained from the thermocouples located on each photothermal panels as indicated by the red spots as shown in Fig. 2c. (c) Temperature vs time heating curves obtained from the thermocouples located inside the wall of PTST at heights of 100 cm, 80 cm, 60 cm, and 30 cm from the bottom of the tunnel, respectively. (d) Thermal energy vs time calculated from the heating curves shown in Fig. 4b. (For interpretation of the references to colour in this figure legend, the reader is referred to the web version of this article.)

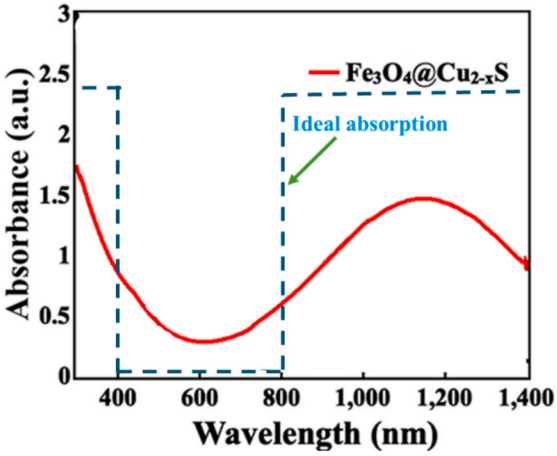


**Fig. 10.** Absorption of $Fe_3O_4@Cu_{2-x}S$ with the ideal pattern indicated by the dashed line.

significant photon-to-heat conversion, enhancing thermal efficiency. This spectral-selective design is consistent with previous reports of hybrid transparent films combining porphyrin compounds and iron oxides for selective solar harvesting and energy generation [16], and similar principles can be applied to optimize AVT and photothermal efficiency in the PTST system. Overall, the seasonal experiments confirm that all PT panels consistently absorb sunlight and contribute to cumulative heating, with observed performance variations primarily attributed to seasonal differences in solar incident angle, ambient temperature, and insulation conditions.

In sharp contrast to the photothermal experiments under simulated solar light [13], the heating curves are significantly affected by the weather and environmental conditions as shown in Figs. 7b and 9b. As shown in these figures, temperature drops coincide with incoming clouds, indicating periods of reduced solar exposure. These fluctuations indicate the sensitive responses of the plasmonic films on the PT panels to direct sunlight availability. However, impressively, the system exhibits strong photothermal effects by maintaining heat even at extremely low temperatures. At ambient temperature – ranging from −5°C to 5°C, the PTST maintains significant heating efficiency. This ability to generate and retain heat highlights the effectiveness of the PT panels in capturing solar radiation.

In Fig. 8b, the average temperatures on top four PT panels remain around 20°C while the top thermocouple registers a temperature ~22°C. These are about 25°C above the ambient temperature (−5°C) with minimum thermal insulation of the solar tunnel. With improved thermal insulation and continued solar harvesting, the interior temperature can be maintained at much higher level (~25°C) for comfort. It should be noted that the initial temperature drops in Fig. 8 are due to moving the system from inside (25°C) to outside (−5°C) of building with a large temperature difference. However, the PT panels soon begin to regain the temperature profiles by heating the structure, demonstrating their effectiveness in compensating for heat losses. This stratification is particularly important in passive heating systems because it suggests that proper airflow management could further enhance heat distribution. The thin polyethylene insulation provided appreciable thermal insulation for reducing heat loss, but incorporating additional insulation layers could further improve the system's efficiency.

The experimental data from Figs. 2 to 9 confirm that the Photothermal Solar Tunnel (PTST) is a highly effective system for capturing and storing solar energy. The system achieves significant temperature gains even under cold conditions, demonstrating its ability to convert solar light into useful heat efficiently, despite variations in sunlight exposure and ambient temperatures. PTST consistently provides strong heating performance, stable thermal retention, and effective stratification of heat within the tunnel.

In the present study, LPD was intentionally not used as a primary variable because measurements remain stable only when the sensor is actively aligned with the sun, whereas standalone measurements exhibit significant temporal variability. Furthermore, direct measurement of LPD within the sealed Photothermal Solar Tunnel is not feasible. Instead, the optical transparency of the photothermal panels, measured independently at approximately 75%, provides a more reliable indicator of the relative light availability across successive panels. This approach allows Fig. 6 to isolate the impact of incident angle and system geometry on thermal performance without conflating these effects with measurement artifacts arising from uncontrolled solar alignment.

In the work by Strušnik el al the authors developed a transparent photothermal coating for window heating, reporting temperature increases under solar illumination while maintaining visible transparency [28]. Their system achieved moderate heating performance under ambient conditions, but did not report extreme winter testing under subzero ambient temperatures. In contrast, our PTST demonstrates a much more aggressive temperature elevation – from –7°C ambient to >30.9°C internal surfaces – under minimal insulation. Thus, our system extends beyond that benchmark in thermal performance under harsh conditions.

Other recent studies on transparent photothermal materials provide further useful points of comparison. For example, Han et al. introduced a transparent photothermal heater based on a soluble NIR-absorbing ionic salt (IDI), achieving over 93% visible transmittance and a photothermal conversion efficiency of ~75% under illumination [29]. While their film shows excellent transparency and conversion, the absolute temperature rise in bulk or integrated heating applications is not directly comparable to tunnel-scale heating systems like ours.

Another relevant work by Guo et al. used a photothermal composite coating ($Cu_7S_4$ nanoparticle-based) on glass, achieving a surface temperature increase of ~17.4°C over ambient under solar illumination, despite only 0.2 wt% nanoparticle loading and maintaining appreciable transparency [30]. Compared to that, our PT panels in the PTST context deliver substantially higher absolute internal temperature rise, under more extreme ambient conditions, thanks to the tunnel architecture and photon-trapping via multiple panels.

The results presented in this study emphasize a system-level photothermal harvesting strategy rather than a re-evaluation of intrinsic absorber optical properties. The $Fe_3O_4@Cu_{2-x}S$ transparent photothermal films used here have been extensively characterized in our prior work, including detailed UV–Vis absorption and transmittance measurements as well as quantitative solar-to-thermal conversion efficiency analysis [13,15]. In particular, multilayer transparent photothermal systems based on these materials were previously shown to achieve solar-to-thermal conversion efficiencies approaching ~60%, with efficiency increasing systematically as additional transparent layers were incorporated [15]. Building on this established materials foundation, the present work demonstrates, for the first time, a three-dimensional photothermal harvesting architecture in which multiple transparent photothermal panels are arranged in parallel within a Photothermal Solar Tunnel (PTST). As solar radiation propagates through the tunnel, each panel partially absorbs and converts light into heat while transmitting the remaining spectrum downstream, resulting in cumulative heat generation along the tunnel length. The measured temperature rises of individual panels under diverse ambient conditions, including winter operation, confirm that effective photothermal conversion occurs at each layer. These findings highlight the capability of transparent multilayer photothermal films to function collectively as a passive, electricity-free solar heating system when integrated into a tunnel geometry, thereby extending photothermal energy harvesting from conventional two-dimensional surfaces to a volumetric, building-integrated configuration.

Viewed alongside existing work, the PTST differs from established passive and solar thermal heating approaches. Traditional passive solar

systems such as Trombe walls and solar air collectors depend on opaque absorbers and thermal mass, which restrict transparency and limit where they can be integrated. Recent studies on transparent or volumetric photothermal absorbers focus mainly on material performance at the panel scale, including porous volumetric receivers and advanced aeromaterials designed for distributed light absorption [31–33]. Standard solar thermal collectors, including flat-plate and evacuated-tube systems, typically require heat-transfer fluids and active components, increasing system complexity [34]. In contrast, the PTST uses multiple transparent photothermal panels arranged in a tunnel to produce cumulative heating while still transmitting visible light, defining a passive, building-integrated heating approach not addressed by existing systems, including semi-transparent PV-T concepts developed for glazing-based applications [35].

## 5. Conclusion

To address critical challenges in solar energy generation for building utility heating, the Photothermal Solar Tunnel (PTST) has been demonstrated as an effective alternative. The PTST system combines high energy conversion efficiency with a structurally simple design that can be readily integrated into both existing and new buildings to support energy-neutral infrastructure. Its unique configuration transforms conventional 2D surface solar harvesting into 3D light transmission through multiple transparent PT panels, significantly increasing the effective solar harvesting area and energy density. Beyond utility heating, the PTST also provides additional illumination in spaces with limited direct sunlight. Unlike traditional PV-based heating systems, which require multiple conversion steps, heavy equipment, and substantial infrastructure, the PTST directly converts solar radiation into heat, offering a lightweight, scalable, and energy-efficient solution.

While the present study demonstrates the feasibility and performance of the PTST system, several limitations remain. In particular, a comprehensive energy-balance model has not yet been developed, and long-term durability under varying environmental conditions has not been fully assessed. Future work will focus on these aspects, including optimization of PT film spectral selectivity (Fig. 10), insulation and heat retention strategies, long-term performance evaluation, and large-scale integration for broader applications in sustainable building design. These efforts will further advance the PTST as a green energy solution that maximizes solar utilization while minimizing complexity and operational costs.

## 6. Data availability

Data available in a publicly accessible repository.

## CRediT authorship contribution statement

**Meher Saketh Gandharapu:** Methodology, Investigation, Data curation. **Anudeep Katepalli:** Data curation. **Anton Harfmann:** Visualization, Funding acquisition. **Mathias Bonmarin:** Validation, Formal analysis. **John Krupczak:** Validation, Formal analysis. **Donglu Shi:** Writing – review & editing, Writing – original draft, Visualization, Validation, Supervision, Resources, Project administration, Methodology, Investigation, Funding acquisition, Formal analysis, Conceptualization.

## Declaration of competing interest

The authors declare that they have no known competing financial interests or personal relationships that could have appeared to influence the work reported in this paper.

## Acknowledgement

We acknowledge the financial support from National Science Foundation CMMI-1953009 and the Michelman Green, Clean and Sustainable Technology Research Innovation Program (F103484). We also acknowledge the financial support from Swiss National Science Foundation with project number: IZSEZ0_223270, titled “Photo-thermal coating for energy efficient windows.

## Data availability

Data will be made available on request.

## References

[1] U.S. Energy Information Administration (EIA), Consumption and Efficiency, retrieved from: https://www.eia.gov/consumption/, accessed: October 2020.
[2] F. Perera, Pollution from fossil-fuel combustion is the leading environmental threat to global pediatric health and equity: solutions exist, Int. J. Environ. Res. 15 (2018) 16.
[3] M.S. Dresselhaus, I.L. Thomas, Alternative energy technologies, Nature 414 (2001) 332–337.
[4] M. Graetzel, Solar energy conversion by dye-sensitized photovoltaic cells, Inor. Chem. 44 (2005) 6842–6851.
[5] R.H. Bube, Photovoltaic Materials, Imperial College Press, London, UK, 1998.
[6] V. Weitbrecht, D. Lehmann, A. Richter, Flow distribution in solar collectors with laminar flow conditions, Sol. Energy 73 (2002) 433–441.
[7] R. Fu, D. Feldman, R. Margolis, M. Woodhouse, K. Ardani, Solar Photovoltaic System Cost Benchmark: Q1 2017, U.S. Department of Energy Office of Scientific and Technical Information, United States, 2017, 10.2172/1395932.
[8] I. Nath, Cleaning up after clean energy: hazardous waste in the solar industry, Stanf. J. Int. Relat. 11 (2010) 6–15.
[9] R. Yang, D. Li, M. Arıcı, S.L. Salazar, Y. Wu, C. Liu, Ç. Yıldız, Spectrally selective nanoparticle–enhanced phase change materials: a study on data–driven optical/thermal properties and application of energy–saving glazing under different climatic conditions, Renew. Sustain. Energy Rev. 186 (2023) 113646, https://doi.org/10.1016/j.rser.2023.113646.
[10] A. García-Sánchez, G. Vallerotto, S. Askins, I. Antón, C. Domínguez, A smart semi–translucent building–integrated PV module based on integrated–tracking micro–concentration providing high power density and active daylight management, Sol. Energy Mater. Sol. Cells 287 (2025) 113246, https://doi.org/10.1016/j.solmat.2024.113246.
[11] M.I. Khan, F. Asfand, S.G. Al-Ghamdi, Progress in research and technological advancements of thermal energy storage systems for concentrated solar power, J. Energy Stor. 55 (Part D) (2022) 105860, https://doi.org/10.1016/j.est.2022.105860. ISSN 2352-152X.
[12] A. Katepalli, Y. Wang, J. Lin, A. Harfmann, M. Bonmarin, J. Krupczak, D. Shi, A photothermal solar tunnel via multiple transparent Fe3O4@Cu2-xS thin films for heating utility application, Solar Energy 271 (2024) 112444, https://doi.org/10.1016/j.solener.2024.112444. ISSN 0038-092X.
[13] M. Lyu, J. Lin, J. Krupczak, D. Shi, Optical thermal insulation via the photothermal effects of Fe3O4 and Fe3O4@Cu2−xS thin films for energy-efficient single-pane windows, MRS Commun. 10 (3) (2020) 439–448.
[14] J. Lin, M. Lyu, D. Shi, 3D solar harvesting and energy generation via multilayers of transparent porphyrin and iron oxide thin films, Energies 16 (2023) 3173, https://doi.org/10.3390/en16073173.
[15] M. Lyu, J. Lin, J. Krupczak, D. Shi, Solar harvesting through multilayer spectral selective iron oxide and porphyrin transparent thin films for photothermal energy generation, Adv. Sustain. Syst. (2021), https://doi.org/10.1002/adsu.202100006.
[16] J. Lin, Y. Wang, M. Lyu, D. Shi, Transparent porphyrin-based hybrid films for spectral selective solar harvesting and energy generation, Sol. Energy Mater. Sol. Cells 243 (2022) 15.
[17] P. Yao, R. Yang, G.H. Qie Sun, X.L. Tang, P. Jin Huan, D. Mu, Transparent photothermal films with high optical selectivity for anti, de-icing, Appl. Thermal Eng. 242 (2024) 122490, https://doi.org/10.1016/j.applthermaleng.2024.122490. ISSN 1359-4311.
[18] W. Li, C. Lin, W. Ma, Y. Li, F. Chu, B. Huang, S. Yao, Transparent selective photothermal coatings for antifogging applications, Cell Rep. Phys. Sci. 2 (5) (2021), https://doi.org/10.1016/j.xcrp.2021.100435, 100435,ISSN 2666-3864.
[19] X. Han, Z. Deng, Z. Yang, Y. Wang, H. Zhu, B. Chen, Z. Cui, R.C. Ewing, D. Shi, Biomarkerless targeting and photothermal cancer cell killing by surface-electrically-charged superparamagnetic Fe3O4 composite nanoparticles, Nanoscale 9 (2017) 1457–1465.
[20] M.E. Donglu Shi, A.W. Sadat, Dunn, D.B. Mast, Photo-fluorescent and magnetic properties of iron oxide nanoparticles for biomedical applications, Nanoscale 7 (18) (2015) 8209–8232.
[21] A. Dunn, S.M. Ehsan, D. Mast, G.M. Pauletti, H. Xu, J. Zhang, R.C. Ewing, D. Shi, Photothermal effects and toxicity of Fe3O4 nanoparticles via near infrared laser irradiation for cancer therapy, Mater. Sci. Eng. C 46 (2015) 97–102.
[22] Y. Zhao, M.E. Sadat, A.W. Dunn, H. Xu, C.-H. Chen, W. Nakasuga, R.C. Ewing, D. Shi, Photothermal effect on Fe3O4 nanoparticles irradiated by white-light for

energy-efficient window applications, Solar Energy Mater Solar Cells. 161 (2017) 247–254.
[23] Y. Zhao, A. Dunn, J. Lin, D. Shi, Photothermal effect of nanomaterials for efficient energy applications, in: Novel Nanomaterials for Biomedical, Environmental and Energy Applications, Elsevier, 2019, pp. 415–434.
[24] M.E. Sadat, M.K. Baghbador, A.W. Dunn, H.P. Wagner, R.C. Ewing, J. Zhang, X. Hong, G.M. Pauletti, D.B. Mast, D. Shi, Photoluminescence and photothermal effect of Fe3O4 nanoparticles for medical imaging and therapy, Appl. Phys. Lett. 105 (9) (2014) 091903.
[25] M. Lyu, J. Lin, D. Shi, Solar desalination via multilayers of transparent photothermal $Fe_3O_4$@Cu2-xS Thin Films, Energ. Technol. 2100590 (2021), https://doi.org/10.1002/ente.202100590.
[26] Q. Tian, J. Hu, Y. Zhu, R. Zou, Z. Chen, S. Yang, R. Li, Q. Su, Y. Han, X. Liu, Sub-10 nm Fe3O4@Cu2−xS core-shell nanoparticles for dual-modal imaging and photothermal Therapy, J. Am. Chem. Soc. 135 (23) (2013) 8571–8577.
[27] J. Lin, D. Shi, Photothermal and photovoltaic properties of transparent thin films of porphyrin compounds for energy applications, Appl. Phys. Rev. 8 (2021) 011302, https://doi.org/10.1063/5.0036961.
[28] D. Strušnik, D. Brandl, H. Schober, J. Ferčec, J. Avsec, A simulation model of the application of the solar STAF panel heat transfer and noise reduction with and without a transparent plate: A renewable energy review, Renew. Sustain. Energy Rev. 134 (2020) 110149, https://doi.org/10.1016/j.rser.2020.110149.
[29] M. Han, B. Kim, H. Lim, H. Jang, E. Kim, Transparent photothermal heaters from a soluble NIR-absorbing diimmonium salt, Adv. Mater. 32 (1) (2020) 1905096, https://doi.org/10.1002/adma.201905096.
[30] W. Guo, C. Liu, N. Li, M. Xi, Y. Che, C. Jiang, S. Zhang, Z. Wang, A highly transparent and photothermal composite coating for effective anti-/de-icing of glass surfaces, Nanoscale Adv. 4 (2022) 2884–2892, https://doi.org/10.1039/D2NA00151A.
[31] J.L. Toroxel, S.M. Silva, A review of passive solar heating and cooling technologies based on bioclimatic and vernacular architecture, Energies 17 (5) (2024) 1006.
[32] Y.-L. He, D. Shen, S. Shen, Advances in porous volumetric solar receivers and enhancement of volumetric absorption, Energy Rev. 2 (3) (2023) 100035.
[33] L.M. Saure, N. Kohlmann, H. Qiu, S. Shetty, A.S. Nia, N. Ravishankar, X. Feng, A. Szameit, L. Kienle, R. Adelung, F. Schütt, ACS Nano 17 (22) (2023) 22444–22455, https://doi.org/10.1021/acsnano.3c05329.
[34] T.V. Kadam, S.Y. Pakhare, A.B. Godse, Performance analysis of solar thermal collectors: A comprehensive review, Measur.: Energy 7 (2025), https://doi.org/10.1016/j.meaene.2025.100059, 100059 ISSN 2950-3450.
[35] A. Samsudin, H. Jarimi, E.Z. Ahmad, S. Shafian, W.F.M. Yusoff, M.M.Z. Makhtar, U. Syafiq, T.R. Razak, S. Yuehong, Recent advances in photovoltaic thermal collectors (PVT): from conventional designs to high insulation glazing and semi-transparent PVT for building applications, J. Build. Eng. 116 (2025) 114500, https://doi.org/10.1016/j.jobe.2025.114500. ISSN 2352-7102.